

## Article

# Microstructural Aspects of the Fabrication of Al/Al<sub>2</sub>O<sub>3</sub> Composite by Friction Stir Processing

Sergey S. Malopheyev , Ivan S. Zuiko , Sergey Yu. Mironov \*  and Rustam O. Kaibyshev

Laboratory of Mechanical Properties of Nanoscale Materials and Superalloys, Belgorod National Research University, Pobeda 85, Belgorod 308015, Russia; malofeev@bsu.edu.ru (S.S.M.); zuiko\_ivan@bsu.edu.ru (I.S.Z.); rustam\_kaibyshev@bsu.edu.ru (R.O.K.)

\* Correspondence: mironov@bsu.edu.ru; Tel.: +7-4722-585456

**Abstract:** The purpose of this work was the examination of microstructural evolution during the fabrication of an Al/Al<sub>2</sub>O<sub>3</sub> composite by friction stir processing (FSP). In order to obtain new insight into this process, a longitudinal section of the produced composite was studied, and advanced characterization techniques (including electron backscatter diffraction and microhardness mapping) were applied. It was found that the reinforcing particles rapidly rearranged into the “onion-ring” structure, which was very stable against the subsequent dispersion. Specifically, the remnants of the comparatively coarse-scale particle agglomerations have survived even after 12 FSP passes. Therefore, it was concluded that three or four FSP passes, which are often applied in practice, are not sufficient to provide a homogeneous dispersion of the reinforcing particles. It was also revealed that the gradual distribution of the nanoscale Al<sub>2</sub>O<sub>3</sub> particles throughout the aluminum matrix promoted a subtle reduction in both the portion of high-angle boundaries and the average grain size. These observations were attributed to the particle pinning of grain-boundary migration and dislocation slip.

**Keywords:** aluminum matrix composite; alumina nanoparticles; friction stir processing; microstructure; texture; electron backscatter diffraction (EBSD)



**Citation:** Malopheyev, S.S.; Zuiko, I.S.; Mironov, S.Y.; Kaibyshev, R.O. Microstructural Aspects of the Fabrication of Al/Al<sub>2</sub>O<sub>3</sub> Composite by Friction Stir Processing. *Materials* **2023**, *16*, 2898. <https://doi.org/10.3390/ma16072898>

Academic Editors: Zhiwei Liu and Peng Xiao

Received: 9 March 2023

Revised: 30 March 2023

Accepted: 4 April 2023

Published: 5 April 2023



**Copyright:** © 2023 by the authors. Licensee MDPI, Basel, Switzerland. This article is an open access article distributed under the terms and conditions of the Creative Commons Attribution (CC BY) license (<https://creativecommons.org/licenses/by/4.0/>).

## 1. Introduction

Aluminum matrix composites offer an attractive synergy of properties, including low density, good strength, and superior thermal stability [1]. Accordingly, these materials are used for high-performance applications in the transportation sector (particularly in the automotive industry), specifically for the manufacturing of pistons, brake rotors, connecting rods, etc. [2]. An important advantage of aluminum matrix composites if compared with other lightweight composites (such as magnesium or titanium-based) is a reasonably low price–performance ratio [3].

Friction stir processing (FSP) is sometimes considered a promising technique for the fabrication of aluminum matrix composites [4–7]. Due to the solid-state nature of this technology, FSP minimizes interfacial reactions between the reinforcing elements and the aluminum matrix and thus provides good interfacial bonding between these two constituents.

The extensive research in this area has conclusively demonstrated the high efficiency of FSP for the fabrication of aluminum matrix composites [4–7]. Specifically, a wide range of composites was successfully produced using a variety of both reinforcing particles and matrix aluminum alloys. The reinforcing elements typically comprise SiC [8–15] or Al<sub>2</sub>O<sub>3</sub> [11,16–25] phases but may also involve other particles [26–33]. On the other hand, the matrix materials included the 1xxx [8,9,16,29], 2xxx [20–22], 5xxx [11,13,27,30,32,33], 6xxx [12,17,23,31], and 7xxx [10,26] series of aluminum alloys.

Moreover, it was found that the agglomeration of the reinforcing particles during FSP represents an essential problem. Specifically, a single FSP pass is usually not suffi-



the conventional FSP reference frame was used, which included FSP direction (PD), normal direction (ND), and transverse direction (TD), as shown in Figure 1a.

To minimize mechanical abrasion of the FSP tool during FSP, the tool was manufactured from a tungsten carbide alloy. The geometry and principal dimensions of the tool are shown in Figure 2a.

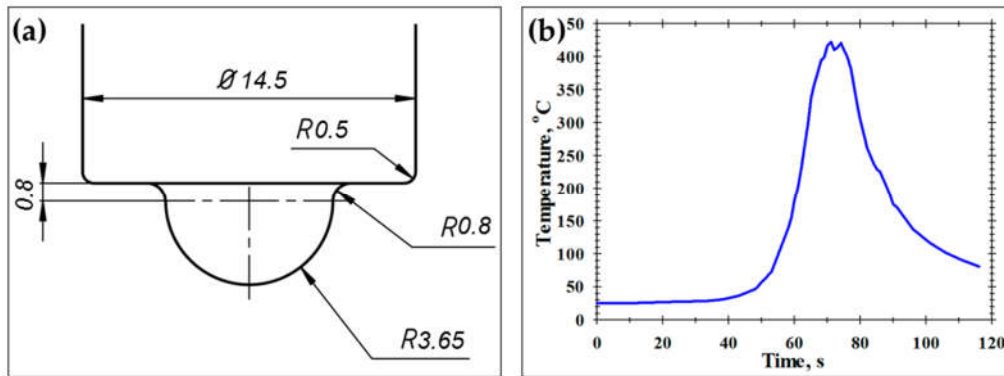


**Figure 2.** (a) Schematic of FSP tool and (b) FSP thermal cycle recorded at the border of the stir zone.

To produce a fine-grained structure in the aluminum matrix, a comparatively low tool rotation rate of 500 rpm was applied. On the other hand, to enhance the dispersion of  $\text{Al}_2\text{O}_3$  powder, the tool translation rate was also selected to be relatively small at 125 mm/min. Hence, the tool advance per rotation was 250  $\mu\text{m}$ .

To examine the effect of multiple passes on microstructural evolution, the workpieces with the preplaced  $\text{Al}_2\text{O}_3$  powder were subjected to 1, 2, 3, 4, 8, and 12 FSP passes using the same processing variables as indicated above. In an attempt to promote a more homogeneous distribution of the reinforcing particles, the upper and bottom parts of the workpieces (as well as their advancing and retreating sides) were inverted between the passes, while the processing direction was kept the same.

To assist the interpretation of microstructural changes, the FSP thermal cycle was recorded employing K-type thermocouples placed at the border of the stir zone at the mid-thickness of an FSP workpiece (Figure 2b). The key characteristics of the recorded temperature profile included a peak temperature of 422 °C and a relatively slow cooling rate.

### 2.3. Microstructural Observations

As discussed in Section 1, microstructural observations in the present work were focused on the longitudinal (PD  $\times$  ND) plane of the stir zone (Figure 1a). The examinations involved optical microscopy, microhardness mapping, and electron backscatter diffraction (EBSD).

In all cases, the FSP'ed workpieces were sectioned in half along the FSP centerline, and metallographic specimens were prepared according to ASTM E3 standards. The final polishing step comprised a long-term (up to 24-h) vibratory polishing with OPS suspension.

The macro-scale structure was studied using optical microscopy and microhardness mapping. The optical observations were conducted using an optical microscope Olympus GX71 equipped with SIAMS 800 software. The Vickers microhardness measurements were performed in accordance with ASTM E92-17 standard by applying a load of 0.2 kg, a dwell time of 10 s, and a step size of 0.25 mm.

The grain structure was investigated by EBSD (the basic principles of EBSD are detailed in Refs. [34,35]) using an FEI Quanta 600 field-emission-gun scanning-electron microscope (SEM) equipped with TSL OIM software. Orientation mapping was conducted employing a scan step size of either 0.5 or 0.25  $\mu\text{m}$ . The low-angle boundaries (LABs) were differentiated from the high-angle boundaries (HABs) using a 15-degree tolerance. The grain size was measured using the equivalent-circle-diameter approach [35].

### 3. Results and Discussion

#### 3.1. Macro-Scale Structure

The evolution of the macro-scale structure within the stir zone as a function of the number of FSP passes is shown in Figure 3. To assist the interpretation of the macro-scale structures, microhardness data were also presented in Figures 4 and 5. Specifically, the microhardness maps in Figure 4 were used for the examination of the spatial distribution of  $\text{Al}_2\text{O}_3$  powder. By analogy with the work by Zhang et al. [36], microhardness profiles were also measured to quantify the dispersion of the reinforcing particles through the matrix material (Figure 5a). Moreover, the average microhardness of the acquired microhardness map was also shown as a function of the number of FSP passes in Figure 5b.

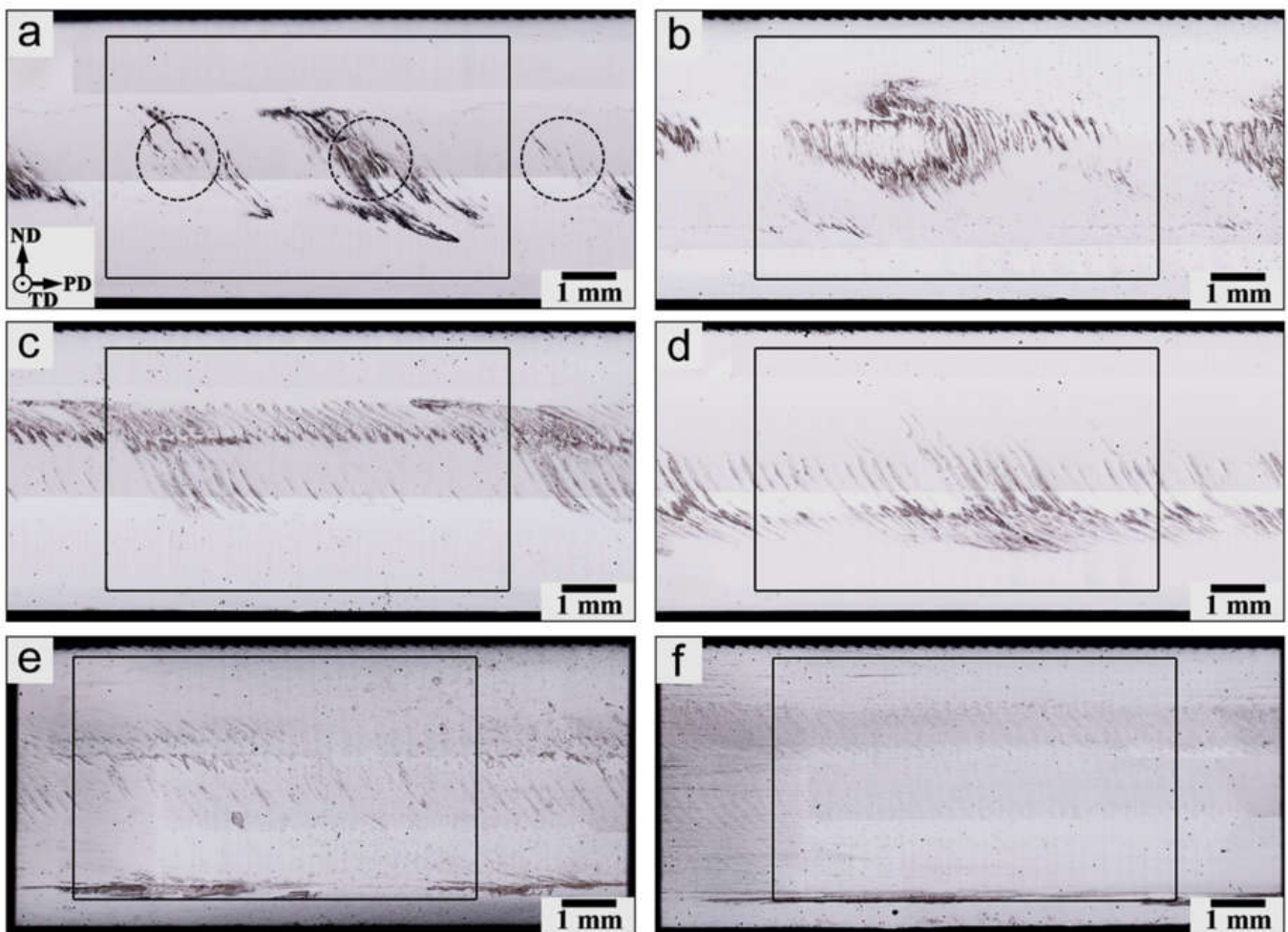


**Figure 3.** Optical images of longitudinal sections of the processed material as a function of the number of FSP passes: (a) 1 pass; (b) 2 passes; (c) 3 passes; (d) 4 passes; (e) 8 passes; and (f) 12 passes. Selected areas outline microhardness maps shown in Figure 4. In (a), circles indicate the approximate positions of the initial placement of alumina powder.

After the first FSP pass, the  $\text{Al}_2\text{O}_3$  powder mainly remained in close proximity to the areas of initial placement (indicated by circles in Figure 3a). The spatial dispersion of the reinforcing particles was fairly limited (Figure 3a), thus giving rise to essential variations in microhardness (Figures 4a and 5a). As a result, the microstructure distribution was fairly non-uniform (Figures 3a and 4a). Hence, a single FSP pass is obviously not sufficient to produce a high-quality composite.

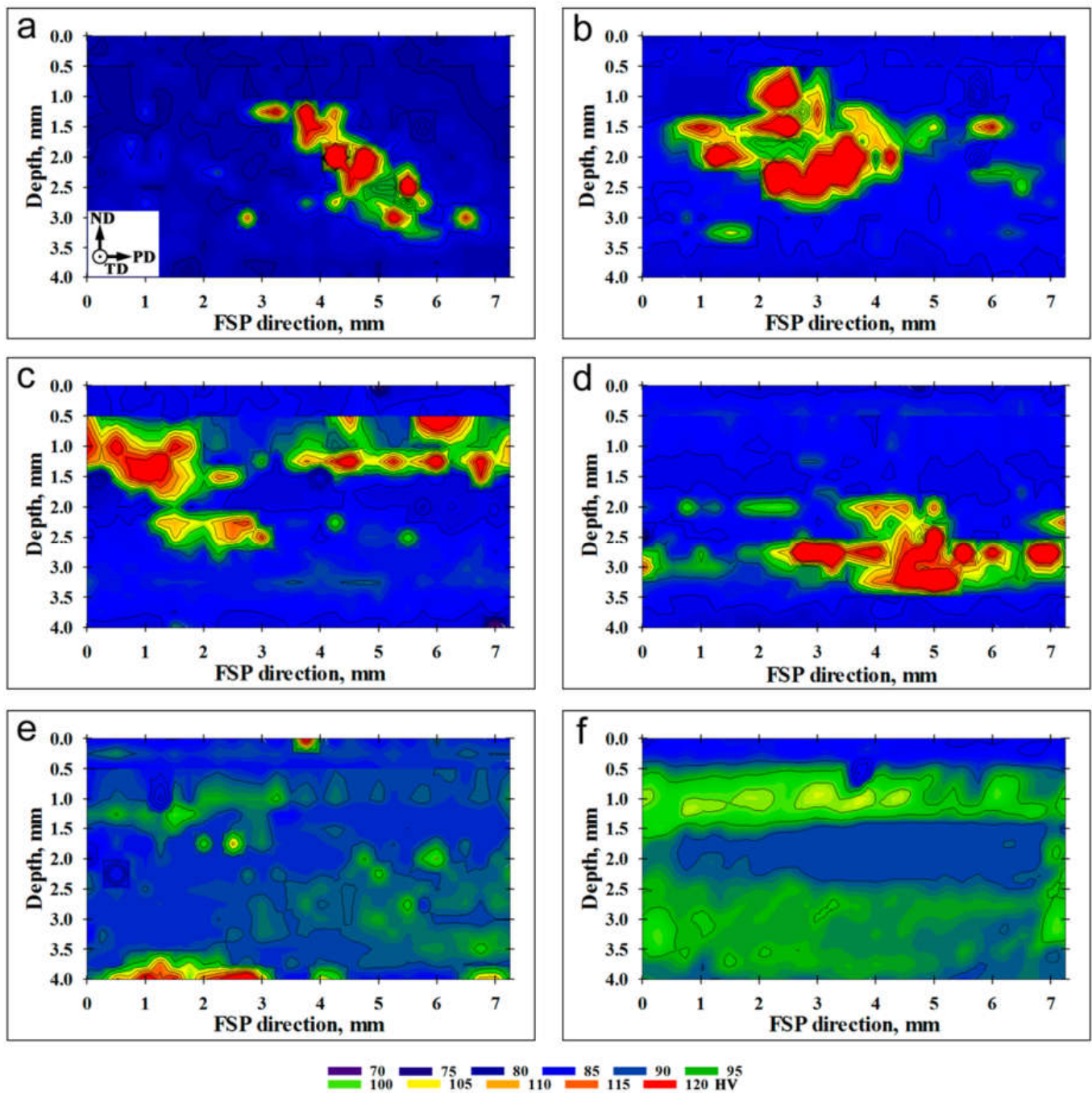


**Figure 4.** Microhardness maps of the processed material as a function of the number of FSP passes: (a) 1 pass; (b) 2 passes; (c) 3 passes; (d) 4 passes; (e) 8 passes; and (f) 12 passes.

Essential particle dispersion in the vertical direction was also worthy of remark (Figure 3a). This observation suggested an extensive vertical material flow within the stir zone.

After two FSP passes, the macro-scale structure became more uniform (compare Figure 3a,b). This resulted in a gradual increase in microhardness (Figure 5b). On the other hand, the reinforcing particles still tended to preferentially concentrate relatively near their initial placement positions (Figure 4b), thereby leading to essential fluctuations in the microhardness profile (Figure 5a).

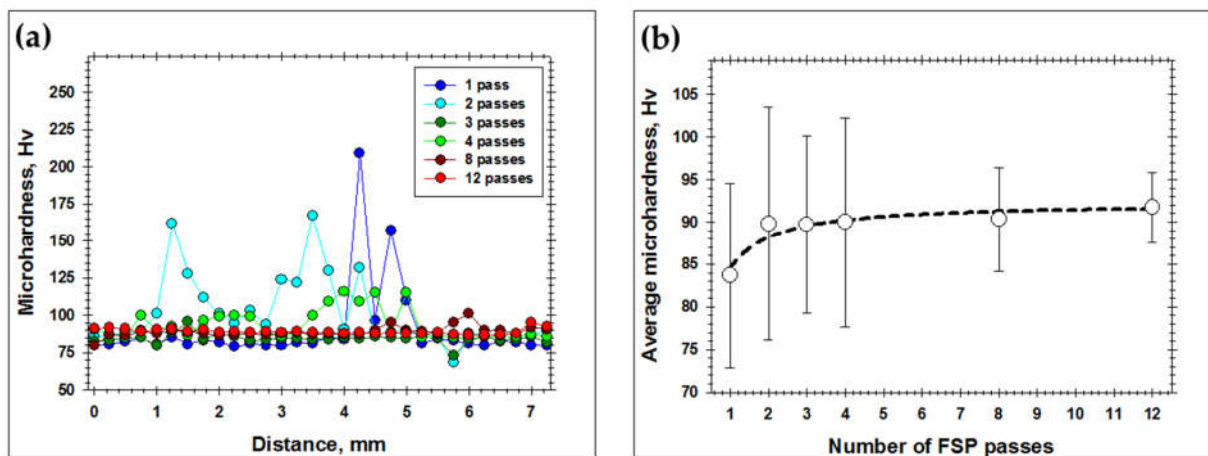


**Figure 5.** Effect of number FSP passes on (a) the microhardness profile measured across the workpieces' mid-thickness and (b) the average microhardness of the acquired microhardness maps. In (b), error bars show the standard deviation. Note: The empty circles in (b) show experimental data points.

The third and fourth FSP passes resulted in the development of a specific structure, which consisted of the regular set of vertically oriented particle-rich bands throughout the stir zone (Figure 3c,d). Importantly, the mean spacing between the bands was close to 250  $\mu\text{m}$ , i.e., virtually the tool advance per revolution. Therefore, the developed structure represented the so-called “onion-ring” structure, which is intrinsic to friction stir welding/processing. In fact, this structure represents a superposition of material layers, which are “cut” from the initial workpiece during every single rotation of the FSP tool [37]. In the present case, the development of the “onion-ring” structure implied the formation of the repeated sequence of the particle-rich and particle-poor layers, i.e., virtually, the development of a new sort of microstructural heterogeneity. The preferential arrangement of the reinforcing particles as the onion-ring structure has been reported in the scientific literature [38–44].

An increased fraction of the reinforcing particles in either the upper or bottom parts of the stir zone was also evident (Figures 3c,d and 4c,d). This observation likely suggested the importance of vertical material flow.

With the further increase in the number of FSP passes, the “onion-ring” structure tended to become less apparent (Figure 3e,f); thus, perhaps evidencing a gradual dispersion of the coarse-scale particle agglomerations. This resulted in a smoothing of microhardness profiles (Figure 5a) and a gradual increase in the average microhardness (Figure 5b). Remarkably, the latter process tended to saturate (Figure 5b).

On the other hand, it is important to emphasize that the agglomerations of  $\text{Al}_2\text{O}_3$  did not disappear completely even after twelve FSP passes (Figure 3f). As a result, the microhardness distribution was still not uniform (Figure 4f). Moreover, the macro-scale cluster of the reinforcing particles at the root of the stir zone also survived after a very large number of FSP passes (Figures 3e,f and 4e).

Thus, even twelve FSP passes are not sufficient to provide an entirely homogeneous distribution of the reinforcing particles.

### 3.2. Grain Structure: FSP without Using Reinforcing Particles

To evaluate the broad aspects of grain structure evolution, a single FSP pass *without* using reinforcing particles was applied. The typical microstructure revealed within the stir zone is shown in Figure 6a.

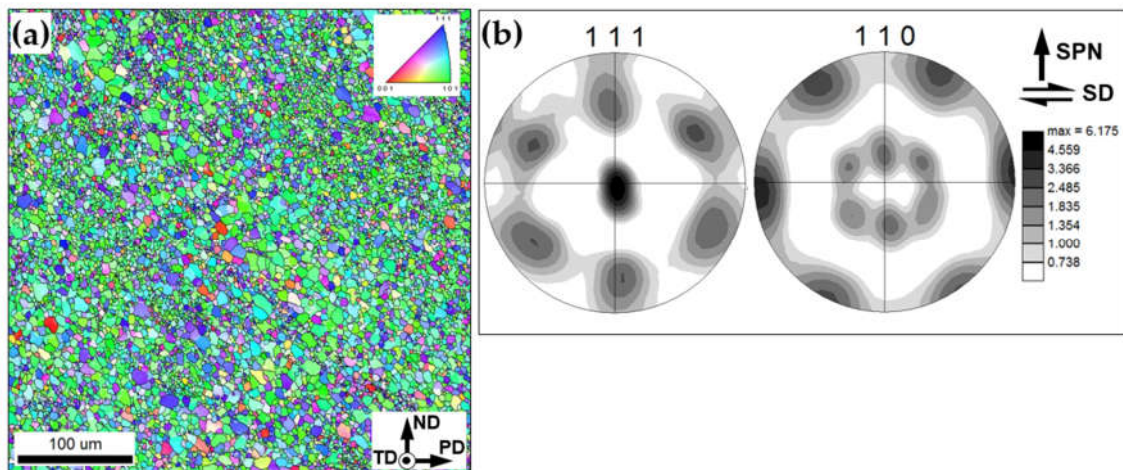


**Figure 6.** Microstructure produced after a single FSP pass without using  $\text{Al}_2\text{O}_3$  powder: (a) EBSD map and (b) 111 and 110 pole figures showing crystallographic texture. In (a), grains are colored according to the transverse direction; LABs and HABs are depicted as white and black lines, respectively. In (b), SD and SPN show the presumed orientations of shear direction and shear plane normal, respectively.

In accordance with expectations, the microstructure was comprised of comparatively-fine grains (with the average grain size being  $\sim 3.5 \mu\text{m}$ ), which contained the essential fraction of LABs. This microstructure is typically revealed in FSP'ed aluminum alloys and is usually attributable to the development of continuous dynamic recrystallization [6,45,46].

Remarkably, the measured HAB fraction ( $\approx 80\%$ ) was somewhat higher than that achievable during continuous recrystallization (60–70% [47,48]). This observation may be indicative of static grain coarsening, which may occur during the FSP cooling cycle [49], due to the relatively low cooling rate (Figure 2b).

To examine crystallographic texture in the stir zone, the measured orientation data were rotated in order to align them with the local geometry of the simple-shear strain within the stir zone [50]. Specifically, to align the shear direction horizontally, the experimental pole figure was rotated by  $90^\circ$  around the normal direction. Then, to align the shear plane normal vertically, the pole figures were additionally tilted by  $60^\circ$  around the transverse direction. The rotated pole figures were shown in Figure 6b. It is seen that the crystallographic texture within the stir zone was dominated by  $B/\bar{B}\{112\} < 110 >$  simple-shear orientation, which is typically observed in friction-stirred aluminum alloys [49,50].

### 3.3. Effect of the Reinforcing $\text{Al}_2\text{O}_3$ Nanoscale Particles on Grain-Structure Evolution

#### 3.3.1. Low-Magnification Overview

A series of low-magnification EBSD orientation maps taken from FSP'ed materials are shown in Figure 7. In the maps, grains are colored according to their crystallographic orientations relative to the transverse direction, while black clusters show pixels with a confidence index below 0.1 (which presumably represent the agglomerations of  $\text{Al}_2\text{O}_3$ ).

It is seen that such clusters are arranged into bands that are oriented nearly vertically (Figure 7a–d), thus resembling the optical microscopy observations (Figure 3). Moreover, in good accordance with optical microscopy, the black clusters tended to disappear with increasing numbers of FSP passes (Figure 7b–f); thus, perhaps evidencing a gradual dispersion of the  $\text{Al}_2\text{O}_3$  particles. Of particular interest was the formation of textural bands after twelve FSP passes (Figure 7f). The possible origin of such bands is considered in Section 3.3.3.

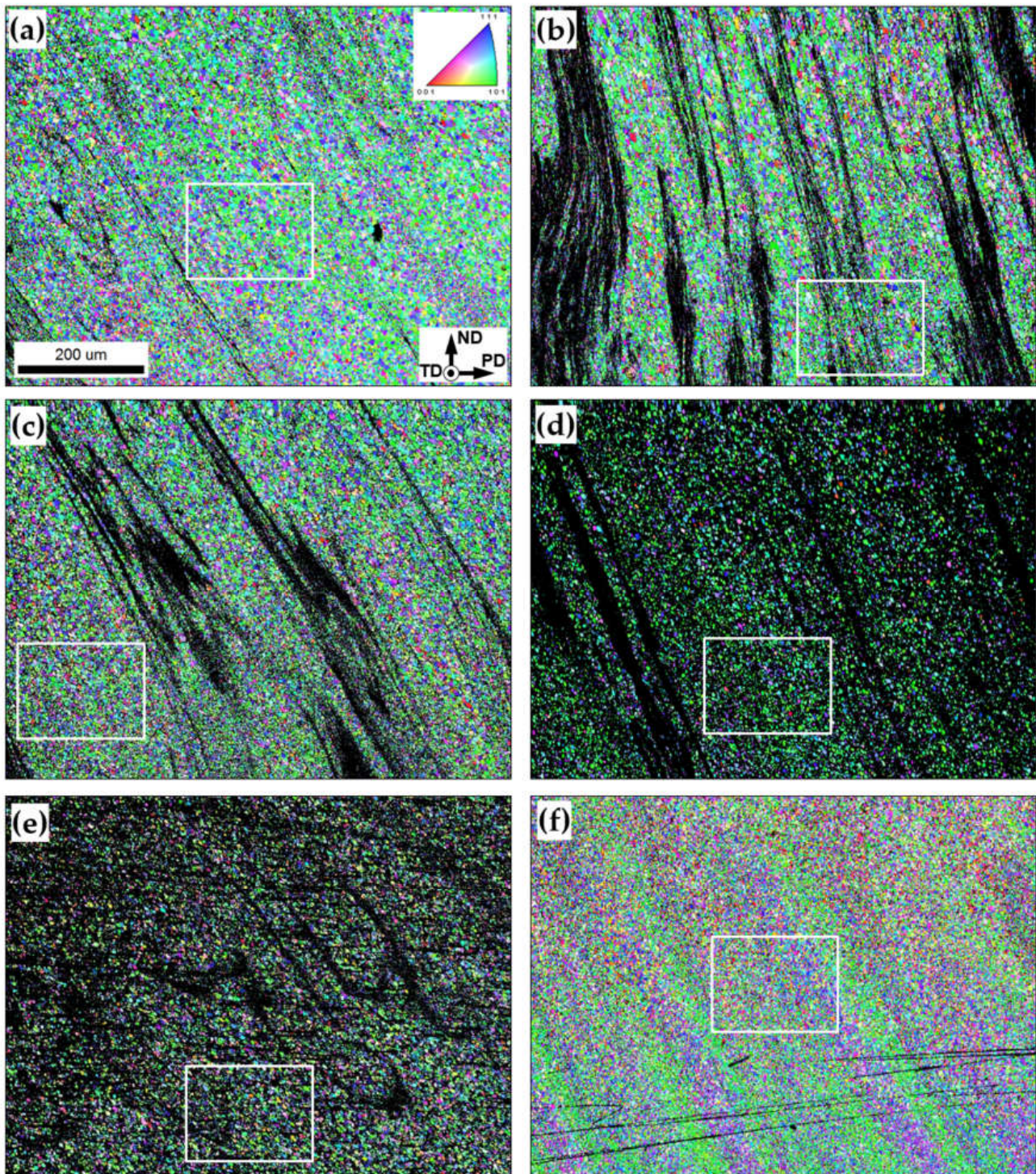


**Figure 7.** Low-magnification EBSD maps showing grain structures of the produced composite as a function of the number of FSP passes: (a) 1 pass; (b) 2 passes; (c) 3 passes; (d) 4 passes; (e) 8 passes; and (f) 12 passes. In the maps, grains are colored according to their crystallographic orientations relative to the transverse direction, while black clusters show the pixels with a confidence index below 0.1. The reference frame and scale of all EBSD maps are indicated in (a). Note: The microstructures within the selected areas (white rectangles) are shown at higher magnification in Figure 7.

### 3.3.2. Microstructure Morphology and Grain Size

In this study, no reliable EBSD data were obtained from the coarse-scale particle-rich bands in Figure 7. Hence, microstructural analysis was focused on the aluminum

matrix. The high-magnification EBSD maps taken from the aluminum matrix after different numbers of FSP passes are shown in Figure 8. In the maps, LABs and HABs are depicted as red and black lines, respectively. The relevant microstructural statistics are given in Figure 9.

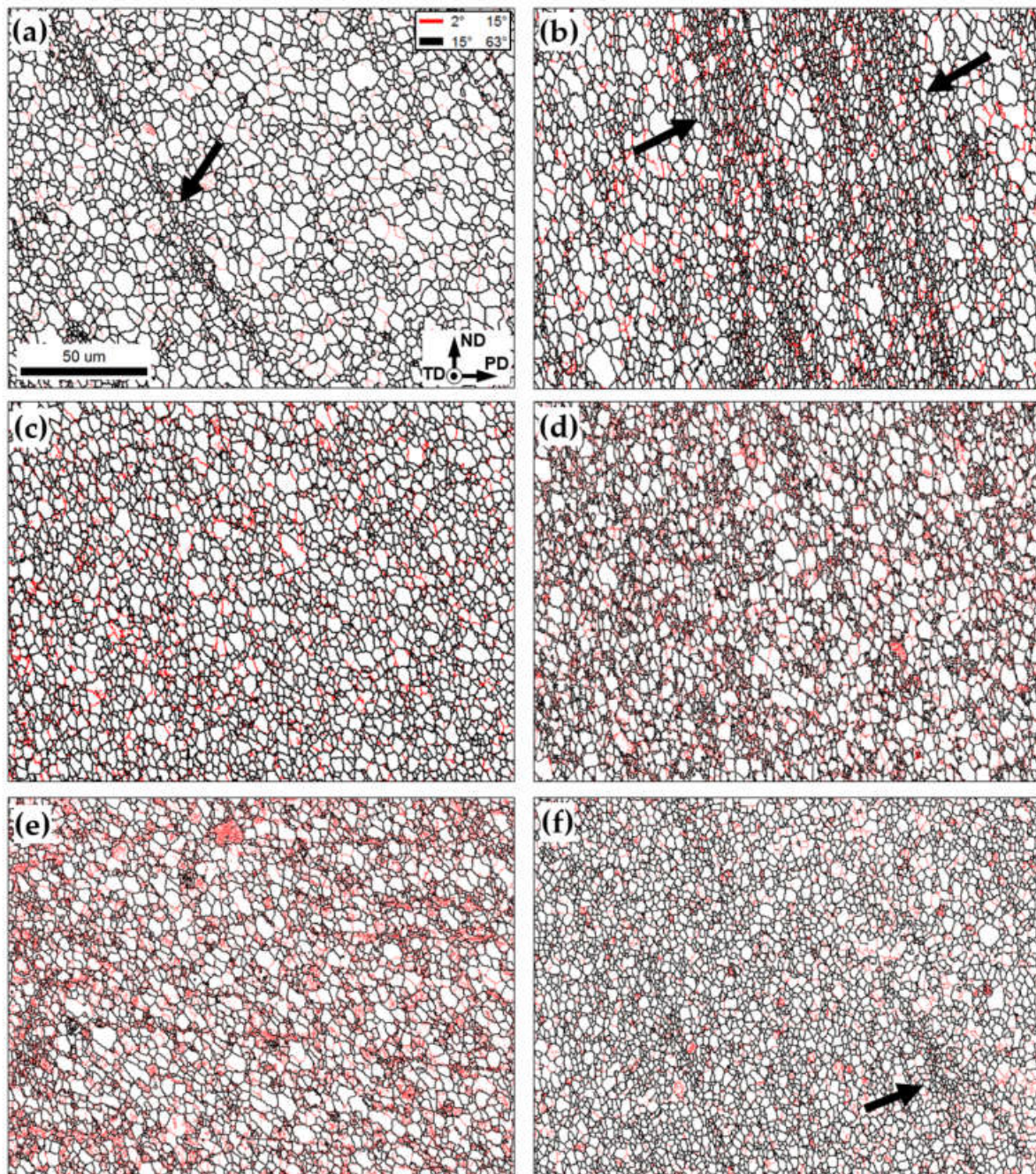


**Figure 8.** High-magnification EBSD grain-boundary maps showing grain structures within the aluminum matrix as a function of the number of FSP passes: (a) 1 pass; (b) 2 passes; (c) 3 passes; (d) 4 passes; (e) 8 passes; and (f) 12 passes. In the maps, LABs and HABs are depicted as red and black lines, respectively. The reference frame and scale of all EBSD maps are indicated in (a). Arrows exemplify the presumed agglomerations of the  $\text{Al}_2\text{O}_3$  powder.

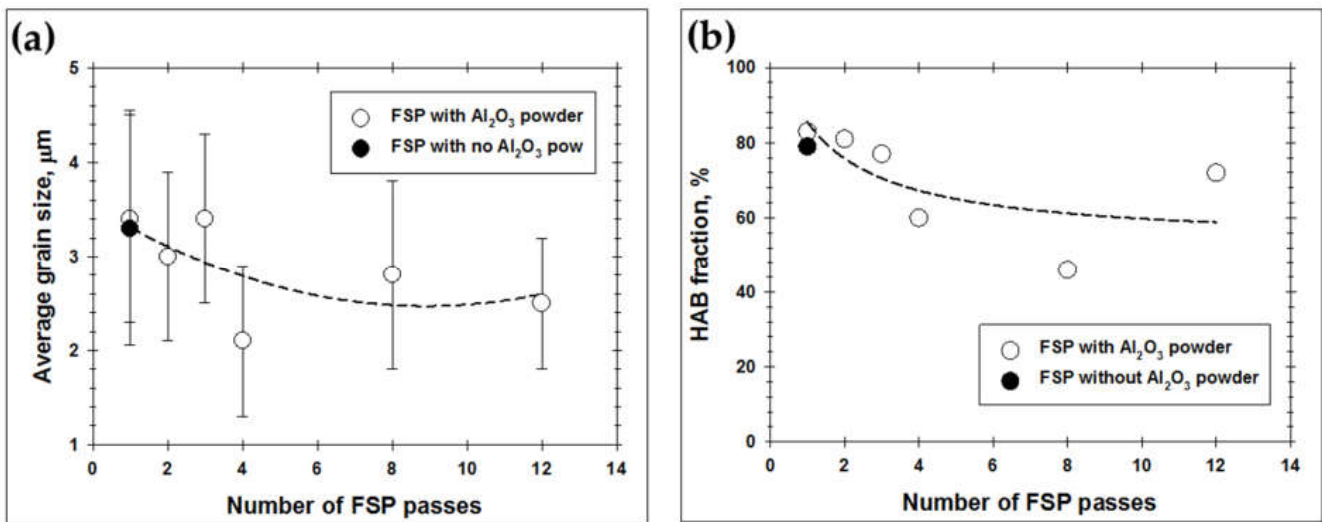


**Figure 9.** Effect of number FSP passes on (a) average grain size and (b) HAB fraction within the aluminum matrix of the produced composite.

After the first and second FSP passes, the important microstructural characteristic was the development of fine-grained bands (arrows in Figure 8a,b). Remarkably, such bands (as well as the adjacent areas) often exhibited increased LAB content (Figure 8b). These observations presumably reflected the influence of the nanoscale  $\text{Al}_2\text{O}_3$  dispersoids.

Specifically, it is known that the relatively small ( $\sim 1 \mu\text{m}$  in size) agglomerations of the nanoscale particles may promote the activation of the mechanism of the particle-stimulated recrystallization [6] and thus promote local grain refinement. On the other hand, the nanoscale dispersoids per se should retard grain-boundary migration and dislocation slip. In the first case, the enhancement of the grain-refinement effect is expected. The second effect may inhibit the progressive evolution of deformation-induced boundaries, including the LAB-to-HAB transformation; this should result in a decreased HAB fraction in the microstructure. It was, therefore, likely that the revealed fine-grained bands were associated with the local concentration of the  $\text{Al}_2\text{O}_3$  particles.

Therefore, the gradual dispersion of the reinforcing particles throughout the aluminum matrix with sequential FSP passes resulted in a steady decrease in both grain size and HAB content (Figures 8c–f and 9a,b). A gradual grain refinement within the matrix of the aluminum-based composites with the number of FSP passes has been reported in the scientific literature [16,17,20,21,51–54].

Remarkably, both above processes tended to saturate, and thus the final effect was comparatively small (Figure 9). Moreover, a significant experimental scattering is worthy of remarking (Figure 9a,b). The latter effect was likely due to the macro-scale inhomogeneity of microstructure distribution, as discussed above.

### 3.3.3. Crystallographic Texture

To investigate the evolution of crystallographic texture, orientation data were derived from EBSD maps in Figure 7 and rotated in a manner described in Section 3.2. The typical examples of rotated pole figures are shown in Figure 10. It is seen that neither the addition of the reinforcing particles nor the number of FSP passes exerted a principal influence on the texture. In all cases, it was dominated by  $B/\bar{B}\{112\} < 110 >$  simple-shear orientations.

Considering the formation of textural bands after 12 FSP passes (Figure 7f), the crystallographic orientations of the bands were also examined. To a first approximation, two different types of textural bands could be defined in Figure 7f: (i) the green and (ii) the blue-to-pink colored ones. The crystallographic orientations of the bands are shown in Figure 11.

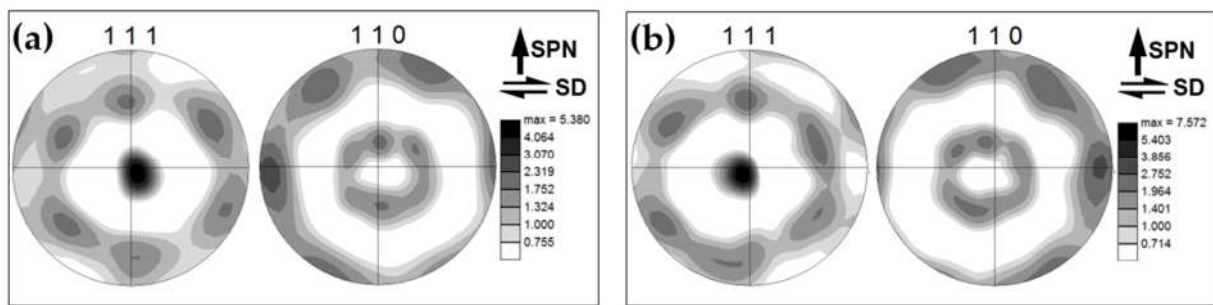


**Figure 10.** Images of 111 and 110 pole figures showing crystallographic texture within the aluminum matrix of the produced composite as a function of the number of FSP passes: (a) 1 pass; (b) 12 passes. SD and SPN show the presumed orientations of shear direction and shear plane normal, respectively.

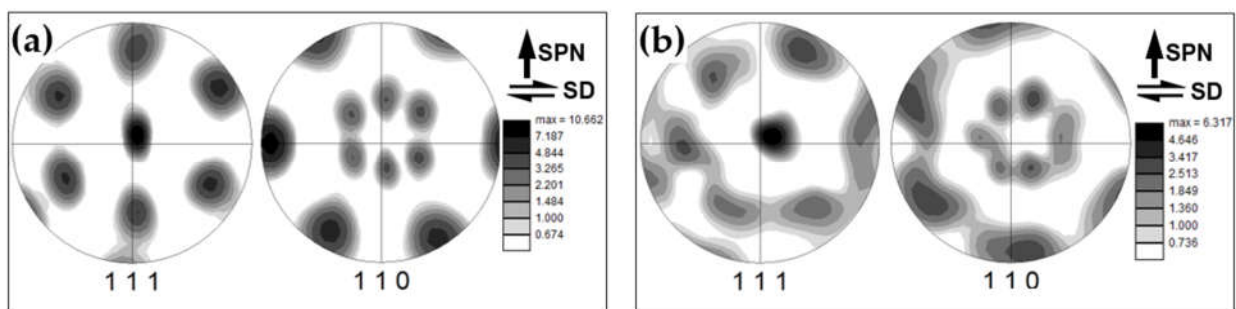


**Figure 11.** Images of 111 and 110 pole figures showing crystallographic orientations of textural bands in the material condition produced after 12 FSP passes (Figure 7f): (a) green-colored bands; and (b) blue-to-pink colored bands. SD and SPN shows the presumed orientations of shear direction and shear plane normal, respectively.

In both cases, those were close to the  $B/\bar{B}\{112\} < 110 >$  texture components. However, in the green-colored bands, the  $< 110 >$  axis was precisely aligned with the transverse direction (i.e., the local shear direction) (Figure 11a), as is normally expected for FSP-induced texture. In the blue-to-pink colored bands, the  $< 110 >$  axis significantly deviated from this direction (Figure 11b). One of the possible explanations for this observation may be the wobbling of the FSP tool.

#### 4. Conclusions

This work was initiated to provide new insight into microstructural evolution during the fabrication of aluminum-matrix composites by FSP. Considering the fact that the reinforcing particles during FSP are usually introduced through the grooves, which are placed along the FSP path, the microstructural examinations in the current study were focused on the longitudinal section of the produced composite. The main conclusions derived from this work are as follows.

- (1) Three or four FSP passes, which are often applied in practice, are not sufficient to provide a homogeneous dispersion of the reinforcing particles throughout the matrix material. It was found that the particles rapidly rearranged into the “onion-ring” structure, which was very stable against the subsequent FSP passes. In fact, the remnants of the “onion-ring” structure as well as the comparatively coarse-scale particle agglomerations in the bottom part of the processed material have survived even after 12 FSP passes.
- (2) The gradual dispersion of the reinforcing particles throughout the aluminum matrix promoted a subtle reduction in grain size and HAB fraction. These observations were suggested to originate from the combined effects of the particle-stimulated

recrystallization as well as the retardation of grain-boundary migration and LAB-to-HAB transformation during FSP.

**Author Contributions:** Conceptualization, S.S.M.; methodology, S.S.M.; software, S.S.M., I.S.Z. and S.Y.M.; validation, S.S.M., I.S.Z., S.Y.M. and R.O.K.; formal analysis, S.S.M.; investigation, S.S.M. and I.S.Z.; resources, S.S.M. and R.O.K.; data curation, S.S.M., I.S.Z. and S.Y.M.; writing—original draft preparation, S.S.M. and S.Y.M.; writing—review and editing, S.Y.M. and R.O.K.; visualization, S.S.M., I.S.Z. and S.Y.M.; supervision, R.O.K.; project administration, S.S.M.; funding acquisition, S.S.M. and I.S.Z. All authors have read and agreed to the published version of the manuscript.

**Funding:** The study was supported by a grant from the Russian Science Foundation No. 21-79-10088 (<https://rscf.ru/en/project/21-79-10088/>; accessed on 3 April 2023).

**Institutional Review Board Statement:** Not applicable.

**Informed Consent Statement:** Not applicable.

**Data Availability Statement:** The data presented in this study are available on request from the corresponding author.

**Acknowledgments:** The experimental works were conducted using equipment of the Joint Research Center of Belgorod State National Research University «Technology and Materials» the activity of which was supported by the Ministry of Science and Higher Education of the Russian Federation within the framework of agreement No. 075-15-2021-690 (the unique identifier for the project is RF—2296.61321X0030).

**Conflicts of Interest:** The authors declare no conflict of interest.

## References

1. Lloyd, D.J. Particle Reinforced Aluminum and Magnesium Matrix Composites. *Int. Mater. Rev.* **1994**, *39*, 1–23. [[CrossRef](#)]
2. Mavhangu, S.T.; Akinlabi, E.T.; Onitiri, M.A.; Varachia, F.M. Aluminum Matrix Composites for Industrial Use: Advances and Trends. *Proc. Manuf.* **2017**, *7*, 178–182. [[CrossRef](#)]
3. Torralba, J.M.; Costa, C.E.; Velasco, F. P/M Aluminum Matrix Composites: An Overview. *J. Mater. Proc. Technol.* **2003**, *133*, 203–206. [[CrossRef](#)]
4. Mishra, R.S.; Ma, Z.Y.; Charit, I. Friction Stir Processing: A Novel Technique for Fabrication of Surface Composite. *Mater. Sci. Eng. A* **2003**, *341*, 307–310. [[CrossRef](#)]
5. Sharma, V.; Prakash, U.; Manoj Kumar, B.V. Surface Composites by Friction Stir Processing: A Review. *J. Mater. Proc. Technol.* **2015**, *224*, 117–134. [[CrossRef](#)]
6. Heidarzadeh, A.; Mironov, S.; Kaibyshev, R.; Cam, G.; Simar, A.; Gerlich, A.P.; Khodabakhshi, A.F.; Mostafaei, A.; Field, D.P.; Robson, J.D.; et al. Friction Stir Welding/Processing of Metals and Alloys: A Comprehensive Review on Microstructural Evolution. *Prog. Mater. Sci.* **2021**, *117*, 100752. [[CrossRef](#)]
7. Gan, Y.X.; Solomon, D.; Reinbolt, M. Friction Stir Processing of Particle Reinforced Composite Materials. *Materials* **2010**, *3*, 329–350. [[CrossRef](#)]
8. Tang, J.; Shen, Y.; Li, J. Influences of Friction Stir Processing Parameters on Microstructure and Mechanical Properties of SiC/Al Composites Fabricated by Multi-Pin Tool. *J. Manuf. Proc.* **2019**, *38*, 279–289. [[CrossRef](#)]
9. Tang, J.; Shen, Y.; Li, J. Investigation of Microstructure and Mechanical Properties of SiC/Al Surface Composites Fabricated by Friction Stir Processing. *Mater. Res. Express* **2019**, *6*, 106576. [[CrossRef](#)]
10. Moustafa, E.B.; Mikhaylovskaya, A.V.; Taha, M.A.; Mosleh, A.O. Improvement of the Microstructure and Mechanical Properties by Hybridizing the Surface of AA7075 by Hexagonal Boron Nitride with Carbide Particles Using the FSP Process. *J. Mater. Res. Technol.* **2022**, *17*, 1986–1999. [[CrossRef](#)]
11. Sahraeinjad, S.; Izadi, H.; Haghshenas, M.; Gerlich, A.P. Fabrication of Metal Matrix Composites by Friction Stir Processing with Different Particles and Processing Parameters. *Mater. Sci. Eng. A* **2015**, *626*, 505–513. [[CrossRef](#)]
12. Huang, C.W.; Aoh, J.N. Friction Stir Processing of Copper-Coated SiC Particulate-Reinforced Aluminum Matrix Composite. *Materials* **2018**, *11*, 599. [[CrossRef](#)]
13. Khodabakhshi, F.; Nosko, M.; Gerlich, A.P. Dynamic Restoration and Crystallographic Texture of a Friction-Stir Processed Al-Mg-SiC Surface Nanocomposite. *Mater. Sci. Technol.* **2018**, *34*, 1773–1791. [[CrossRef](#)]
14. Wojcicka, A.; Mroczka, K.; Kurtyka, P.; Binkowski, M.; Wrobel, Z. X-ray Microtomography Analysis of the Aluminum Alloy Composite Reinforced by SiC after Friction Stir Processing. *J. Mater. Eng. Perform.* **2014**, *23*, 3215–3221. [[CrossRef](#)]
15. Wang, W.; Shi, Q.; Liu, P.; Li, H.; Li, T. A Novel Way to Produce Bulk SiCp Reinforced Aluminum Metal Matrix Composites by Friction Stir Processing. *J. Mater. Proc. Technol.* **2009**, *209*, 2099–2103. [[CrossRef](#)]

16. Orłowska, M.; Pixner, F.; Hutter, A.; Enzinger, N.; Olejnik, L.; Lewandowska, M. Manufacturing of Coarse and Ultrafine-Grained Aluminum Matrix Composites Reinforced with Al<sub>2</sub>O<sub>3</sub> Nanoparticles via Friction Stir Processing. *J. Manuf. Proc.* **2022**, *80*, 359–373. [[CrossRef](#)]
17. Shafiei-Zarghani, A.; Kashani-Bozorg, S.F.; Zarei-Hanzaki, A. Wear Assessment of Al/Al<sub>2</sub>O<sub>3</sub> Nanocomposite Surface Layer Produced Using Friction Stir Processing. *Wear* **2011**, *270*, 403–412. [[CrossRef](#)]
18. Du, Z.; Tan, M.J.; Guo, J.F.; Bi, G.; Wei, J. Fabrication of a New Al-Al<sub>2</sub>O<sub>3</sub>-CNTs Composite Using Friction Stir Processing (FSP). *Mater. Sci. Eng. A* **2016**, *667*, 125–131. [[CrossRef](#)]
19. Eskandari, H.; Taheri, R.; Khodabakhshi, F. Friction-Stir Processing of an AA8026-TiB<sub>2</sub>-Al<sub>2</sub>O<sub>3</sub> Hybrid Nanocomposite. *Mater. Sci. Eng. A* **2016**, *660*, 84–96. [[CrossRef](#)]
20. Moustafa, E. Effect of Multi-Pass Friction Stir Processing on Mechanical Properties for AA2024/Al<sub>2</sub>O<sub>3</sub> Nanocomposites. *Materials* **2017**, *10*, 1053. [[CrossRef](#)]
21. AbuShanab, W.S.; Moustafa, E.B. Effects of Friction Stir Processing Parameters on the Wear Resistance and Mechanical Properties of Fabricated Metal Matrix Nanocomposites (MMNCs) Surface. *J. Mater. Res. Technol.* **2020**, *9*, 7460–7471. [[CrossRef](#)]
22. Moustafa, E.B. Dynamic Characteristics Study for Surface Composite of AMMNCs Matrix Fabricated by Friction Stir Process. *Materials* **2018**, *11*, 1240. [[CrossRef](#)] [[PubMed](#)]
23. Shafiei-Zarghani, A.; Kashani-Bozorg, S.F.; Zarei-Hanzaki, A. Microstructures and Mechanical Properties of Al/Al<sub>2</sub>O<sub>3</sub> Surface Nano-Composite Layer Produced by Friction Stir Processing. *Mater. Sci. Eng. A* **2009**, *500*, 84–91. [[CrossRef](#)]
24. Mazaheri, Y.; Karimzadeh, F.; Enayati, M.H. A Novel Technique for Development of A356/Al<sub>2</sub>O<sub>3</sub> Surface Nanocomposite by Friction Stir Processing. *J. Mater. Proc. Technol.* **2011**, *211*, 1614–1619. [[CrossRef](#)]
25. Mazaheri, Y.; Karimzadeh, F.; Enayati, M.H. Tribological Behavior of A356/Al<sub>2</sub>O<sub>3</sub> Surface Nanocomposite Prepared by Friction Stir Processing. *Metall. Mater. Trans. A* **2014**, *45*, 2250–2259. [[CrossRef](#)]
26. Rana, H.; Badheka, V. Influence of Friction Stir Processing Conditions on the Manufacturing of Al-Mg-Zn-Cu Alloy/Boron Carbide Surface Composite. *J. Mater. Proc. Technol.* **2018**, *255*, 795–807. [[CrossRef](#)]
27. Pariyar, A.; Perugu, C.; Toth, L.; Kailas, S. Microstructure and Mechanical Behavior of Polymer-Derived in-Situ Ceramic Reinforced Lightweight Aluminum Matrix Composite. *J. Alloy. Compd.* **2021**, *880*, 160430. [[CrossRef](#)]
28. Sharma, A.; Gupta, G.; Paul, J. A Comprehensive Review on the Dispersion and Survivability Issues of Carbon Nanotubes in Al/CNT Nanocomposites Fabricated via Friction Stir Processing. *Carbon Lett.* **2021**, *31*, 339–370. [[CrossRef](#)]
29. Mahmoud, E.R.I.; Tash, M.M. Characterization of Aluminum-Based-Surface Matrix Composites with Iron and Iron Oxide Fabricated by Friction Stir Processing. *Materials* **2016**, *23*, 505. [[CrossRef](#)]
30. Papantoniou, I.G.; Markopoulos, A.P.; Manolakos, D.E. A New Approach in Surface Modification and Surface Hardening of Aluminum Alloys Using Friction Stir Process: Cu-Reinforced AA5083. *Materials* **2020**, *13*, 1278. [[CrossRef](#)]
31. Guo, L.; Liu, Y.; Shen, K.; Song, C.; Yang, M.; Kim, K.; Wang, W. Enhancing Corrosion and Wear Resistance of AA6061 by Friction Stir Processing with Fe<sub>78</sub>Si<sub>9</sub>B<sub>13</sub> Glass Particles. *Materials* **2015**, *8*, 5084–5097. [[CrossRef](#)] [[PubMed](#)]
32. Rubtsov, V.; Chumaevskii, A.; Gusarova, A.; Knyazhev, E.; Gurianov, D.; Zykova, A.; Kalashnikova, T.; Cheremnov, A.; Savchenko, N.; Vorontsov, A.; et al. Macro- and Microstructure of In-Situ Composites Prepared by Friction Stir Processing of AA5056 Admixed with Copper Powders. *Materials* **2023**, *16*, 1070. [[CrossRef](#)]
33. Chumaevskii, A.; Zykova, A.; Sudarikov, A.; Knyazhev, E.; Savchenko, N.; Gubanov, A.; Moskvichev, E.; Gurianov, D.; Nikolaeva, A.; Vorontsov, A.; et al. In-Situ Al-Mg Alloy Base Composite Reinforced by Oxides and Intermetallic Compounds Resulted from Decomposition of ZrW<sub>2</sub>O<sub>8</sub> during Multipass Friction Stir Processing. *Materials* **2023**, *16*, 817. [[CrossRef](#)]
34. Adams, B.L.; Wright, S.I.; Kunze, K. Orientation imaging: The Emergence of a New Microscopy. *Metal. Trans. A* **1993**, *24*, 819–831. [[CrossRef](#)]
35. Humphreys, F.J. Quantitative Metallography by Electron Back-Scattered Diffraction. *J. Microsc.* **1999**, *195*, 170–185. [[CrossRef](#)]
36. Zhang, C.; Hu, X.; Lu, P. Fatigue and Hardness Effects of a Thin Buffer Layer on the Heat Affected Zone of a Weld Repaired Bisplate80. *J. Mater. Proc. Technol.* **2012**, *212*, 393–401. [[CrossRef](#)]
37. Krishnan, K.N. On the Formation of Onion Rings in Friction Stir Welds. *Mater. Sci. Eng. A* **2002**, *327*, 246–251. [[CrossRef](#)]
38. Abraham, S.J.; Dinaharan, I.; Selvam, J.D.R.; Akinlabi, E.T. Microstructural Characterization of Vanadium Particles Reinforced AA6063 Aluminum Matrix Composites via Friction Stir Processing with Improved Tensile Strength and Appreciable Ductility. *Compos. Commun.* **2019**, *12*, 54–58. [[CrossRef](#)]
39. Khan, M.; Rehman, A.; Aziz, T.; Naveed, K.; Ahmad, I.; Subhani, T. Cold Formability of Friction Stir Processed Aluminum Composites Containing Carbon Nanotubes and Boron Carbide Particles. *Mater. Sci. Eng. A* **2017**, *701*, 382–388. [[CrossRef](#)]
40. Arab, S.M.; Karimi, S.; Jahromi, S.A.J.; Javadpour, S.; Zebarjad, S.M. Fabrication of Novel Fiber Reinforced Aluminum Composites by Friction Stir Processing. *Mater. Sci. Eng. A* **2015**, *632*, 50–57. [[CrossRef](#)]
41. Jeon, C.H.; Jeong, Y.H.; Seo, J.J.; Tien, H.N.; Hong, S.T.; Yum, Y.J.; Hur, S.H.; Lee, K.J. Material Properties of Graphene/Aluminum Metal Matrix Composites Fabricated by Friction Stir Processing. *Int. J. Precis. Eng. Manuf.* **2014**, *15*, 1235–1239. [[CrossRef](#)]
42. Liu, Q.; Ke, L.; Liu, F.; Huang, C.; Xing, L. Microstructure and Mechanical Property of Multi-Walled Carbon Nanotubes Reinforced Aluminum Matrix Composites Fabricated by Friction Stir Processing. *Mater. Des.* **2013**, *45*, 343–348. [[CrossRef](#)]
43. Lee, I.S.; Hsu, C.J.; Chen, C.F.; Ho, N.J.; Kao, P.W. Particle-Reinforced Aluminum Matrix Composites Produced from Powder Mixtures via Friction Stir Processing. *Compos. Sci. Technol.* **2011**, *71*, 693–698. [[CrossRef](#)]

44. Nakama, D.; Katoh, K.; Tokisue, H. Effect of Probe Shape on Dispersibility of Alumina Particles into 6061 Aluminum Alloy by Friction Stir Processing. *J. Jap. Inst. Light Metal.* **2011**, *61*, 95–99. [[CrossRef](#)]
45. Fonda, R.W.; Bingert, J.F.; Colligan, K.J. Development of Grain Structure during Friction Stir Welding. *Scripta Mater.* **2004**, *51*, 243–248. [[CrossRef](#)]
46. Mironov, S.; Inagaki, K.; Sato, Y.S.; Kokawa, H. Effect of Welding Temperature on Microstructure of Friction-Stir Welded Aluminum Alloy. *Metall. Mater. Trans. A* **2015**, *46*, 783–790. [[CrossRef](#)]
47. Humphreys, F.J.; Prangnell, P.B.; Bowen, J.R.; Gholinia, A.; Harris, C. Developing Stable Fine-Grain Microstructures by Large Strain Deformation. *Philos. Trans. R. Soc. Lond. A* **1999**, *357*, 1663–1681. [[CrossRef](#)]
48. Prangnell, P.B.; Bowen, J.R.; Apps, P.J. Ultra-Fine Grain Structures in Aluminum Alloys by Severe Plastic Deformation Processing. *Mater. Sci. Eng. A* **2004**, *375–377*, 178–185. [[CrossRef](#)]
49. Prangnell, P.B.; Heason, C.P. Grain Structure Formation during Friction Stir Welding Observed by the “Stop Action Technique”. *Acta Mater.* **2005**, *53*, 3179–3192. [[CrossRef](#)]
50. Fonda, R.W.; Knipling, K.E. Texture Development in Friction Stir Welds. *Sci. Technol. Weld. Join.* **2011**, *16*, 288–294. [[CrossRef](#)]
51. Moustafa, E.B.; AbuShanab, W.S.; Ghandourah, E.; Taha, M.A. Microstructural, Mechanical and Thermal Properties Evaluation of AA6061/Al<sub>2</sub>O<sub>3</sub>-BN Hybrid and Mono Nanocomposite Surface. *J. Mater. Res. Technol.* **2020**, *9*, 15486–15495. [[CrossRef](#)]
52. Moustafa, E.B.; Melaibari, A.; Alsoruji, G.; Khalil, A.M.; Mosleh, A.O. Tribological and Mechanical Characteristics of AA5083 Alloy Reinforced by Hybridising Heavy Ceramic Particles Ta<sub>2</sub>C & VC with Light GNP and Al<sub>2</sub>O<sub>3</sub> Nanoparticles. *Ceramic Int.* **2022**, *48*, 4710–4721. [[CrossRef](#)]
53. Moustafa, E.B.; Abushanab, W.S.; Melaibari, A.; Yakovtseva, O.; Mosleh, A.O. The Effectiveness of Incorporating Hybrid Reinforcement Nanoparticles in the Enhancement of the Tribological Behavior of Aluminum Metal Matrix Composites. *JOM* **2021**, *73*, 4338–4348. [[CrossRef](#)]
54. Abushanab, W.S.; Moustafa, E.B.; Melaibari, A.A.; Kotov, A.D.; Mosleh, A.O. A Novel Comparative Study Based on the Economic Feasibility of the Ceramic Nanoparticles Role’s in Improving the Properties of the AA5250 Nanocomposites. *Coatings* **2021**, *11*, 977. [[CrossRef](#)]

**Disclaimer/Publisher’s Note:** The statements, opinions and data contained in all publications are solely those of the individual author(s) and contributor(s) and not of MDPI and/or the editor(s). MDPI and/or the editor(s) disclaim responsibility for any injury to people or property resulting from any ideas, methods, instructions or products referred to in the content.